

Clusters containing open-shell molecules. III. Quantum five-dimensional/two-surface bound-state calculations on Ar n OH van der Waals clusters ($X^2\Pi$, $n=4$ to 12)

Minzhong Xu, Zlatko Bačić, and Jeremy M. Hutson

Citation: *The Journal of Chemical Physics* **117**, 4787 (2002); doi: 10.1063/1.1497967

View online: <http://dx.doi.org/10.1063/1.1497967>

View Table of Contents: <http://scitation.aip.org/content/aip/journal/jcp/117/10?ver=pdfcov>

Published by the [AIP Publishing](#)

Articles you may be interested in

[Symmetry-adapted perturbation theory based on unrestricted Kohn-Sham orbitals for high-spin open-shell van der Waals complexes](#)

J. Chem. Phys. **137**, 164104 (2012); 10.1063/1.4758455

[A new potential energy surface for OH\(\$A^2\Sigma^+\$ \)–Kr: The van der Waals complex and inelastic scattering](#)

J. Chem. Phys. **137**, 154305 (2012); 10.1063/1.4757859

[Ar \$n\$ HF van der Waals clusters revisited. I. New low-energy isomeric structures for \$n=6\$ –13](#)

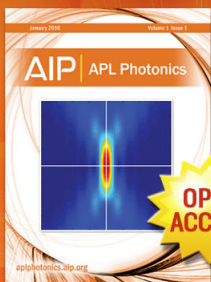
J. Chem. Phys. **121**, 11045 (2004); 10.1063/1.1811612

[Potential energy surfaces and bound states for the open-shell van der Waals cluster Br–HF](#)

J. Chem. Phys. **119**, 8873 (2003); 10.1063/1.1615238

[Clusters containing open-shell molecules. II. Equilibrium structures of Ar \$n\$ OH Van der Waals clusters \(\$X^2\Pi\$, \$n=1\$ to 15\)](#)

J. Chem. Phys. **117**, 4777 (2002); 10.1063/1.1497966



Launching in 2016!

The future of applied photonics research is here

OPEN
ACCESS

AIP | APL
Photonics

Clusters containing open-shell molecules. III. Quantum five-dimensional/two-surface bound-state calculations on Ar_nOH van der Waals clusters ($X^2\Pi$, $n=4$ to 12)

Minzhong Xu and Zlatko Bačić^{a)}

Department of Chemistry, New York University, New York, New York 10003

Jeremy M. Hutson^{b)}

Department of Chemistry, University of Durham, South Road, Durham, DH1 3LE, England

(Received 1 May 2002; accepted 12 June 2002)

This paper presents a theoretical study of the bound states of the open-shell OH radical in its ground electronic state ($X^2\Pi$) interacting with n Ar atoms, for n from 4 to 12. After freezing the geometry of the Ar_n cage or subunit at the equilibrium structure (preceding paper), we carry out nonadiabatic five-dimensional quantum dynamics calculations on two coupled potential energy surfaces, using an extension of the method previously applied to closed-shell Ar_nHF clusters [J. Chem. Phys. **103**, 1829 (1995)]. The method is based on a discrete variable representation (DVR) for the translational motion of OH relative to Ar_n , combined with a finite basis representation of the OH hindered rotation and electronic structure, including spin-orbit effects. The pattern of OH hindered rotor levels in clusters is similar to that in Ar-OH itself, though extended over three to four times the energy range for $n=4$ to 9. Ar_{12}OH has a nearly spherical shell of Ar atoms around the OH, so the anisotropic splitting is very small. For $n=10$ and 11, the anisotropy may be viewed as arising from holes in an otherwise spherical shell, and the resulting patterns of hindered rotor levels are inverted versions of those for Ar_2OH and Ar-OH. © 2002 American Institute of Physics.
[DOI: 10.1063/1.1497967]

I. INTRODUCTION

Clusters containing a central molecule surrounded by solvent atoms provide important prototypes for solvation processes. Those containing open-shell molecules are particularly interesting because they are models for the solvation of reactive species and reaction intermediates. The range of structures available for such species is considerably richer than for single-component clusters, or even for closed-shell heteroclusters such as Ar_nHF .¹

In previous work, we have explored the structures of Ar_nCH (paper I)² and Ar_nOH clusters (Paper II)³ by performing simulated annealing calculations on surfaces that take account of the open-shell character and include spin-orbit coupling. Substantially different structures were found in the two cases. For Ar_nCH , because the $X^2\Pi$ state of CH has a π^1 configuration, the Ar-CH interaction potential strongly favors approach of an Ar atom in the nodal plane of the singly occupied π orbital.⁴ This was found to have important consequences for the Ar_nCH structures: a persistent coplanar Ar_2CH motif was observed, and the Ar cages formed around CH ($X^2\Pi$) were found to be strongly distorted.² Ar_nOH clusters were found to be quite different, because the $X^2\Pi$ state of OH has a π^3 configuration, so that the in-plane approach of an Ar atom is much less strongly favored. The interaction potential for Ar-OH ($X^2\Pi$) has a minimum at

the near-linear Ar-HO geometry.⁵⁻⁷ As a result, the structures of the Ar_nOH clusters are much less distorted³ than those for Ar_nCH .²

Spectra of Ar_nOH clusters could be observed by methods similar to those used for Ar-OH,⁸ including laser induced fluorescence (LIF),⁹⁻¹² stimulated emission pumping (SEP),¹³⁻¹⁵ microwave spectroscopy,¹⁶ and direct infrared absorption¹⁷ in supersonic jets. For any of these, the intensity is carried primarily by the OH monomer and the most intense bands will be those involving OH libration (blocked translation) or hindered rotation. In this paper, we will calculate the frequencies of such bands in clusters by performing five-dimensional quantum bound-state calculations, holding the Ar cage fixed at the geometry of a minimum (global or local) and allowing the OH molecule to translate and rotate within it. The theory needed for such calculations will be described below. The calculations will include both potential energy surfaces arising from OH ($X^2\Pi$) and the coupling between them as well as spin-orbit effects.

A particularly interesting prospect is the observation of Ar_nOH clusters in liquid helium droplets. For Ar_nHF clusters, such experiments¹⁸ have succeeded in resolving size-selected clusters for n up to 9, and in observing multiple structural isomers for $n > 3$.

Open-shell clusters show new effects that are not seen for closed-shell clusters. In particular, the existence of an angular momentum about the diatom axis has profound effects for the hindered rotor levels, because it allows odd-order terms in the Legendre (or spherical harmonic) expansion of the potential to have nonzero diagonal matrix

^{a)} Author to whom correspondence should be addressed. Electronic mail: zlatko.bacic@nyu.edu

^{b)} Electronic mail: j.m.hutson@durham.ac.uk

elements in the free-rotor basis set. In addition, there are effects stemming from the existence of multiple potential energy surfaces and from spin-orbit coupling.

The methodology needed to carry out five-dimensional (5D) computations on closed-shell systems such as Ar_nHF has been developed by Bačić and co-workers.^{19–21} In the present paper, we extend this approach to treat an open-shell radical such as OH ($X^2\Pi$) interacting with an Ar_n subunit. In Sec. II we describe the theory and computational aspects of the rovibrational calculations and in Sec. III we present our results for cluster sizes from $n=4$ –12. Our conclusions are in Sec. IV.

II. THEORY AND COMPUTATIONAL ASPECTS

A. Notation

We use the notation of Dubernet, Flower, and Hutson²² for clusters containing open-shell species. All quantum numbers and other quantities that are conventionally denoted by upper-case letters for diatomic molecules are replaced by lower-case letters for the monomer in a cluster, and the corresponding upper-case letters are reserved for the complex as a whole.

For a $^2\Pi$ molecule in Hund case (a), the total electron orbital angular momentum \mathbf{I} and the total electron spin \mathbf{s} of the diatomic monomer are strongly coupled to the monomer axis \mathbf{r} , with projections λ and σ , respectively. The total projection is $\omega=\lambda+\sigma$. We use the convention that the OH monomer axis \mathbf{r} runs from O to H. The angular momentum due to rotation of the monomer is perpendicular to \mathbf{r} , so that ω is also the projection of the total monomer angular momentum \mathbf{j} onto \mathbf{r} . In OH ($X^2\Pi$), $|\omega|$ can take values $\frac{1}{2}$ and $\frac{3}{2}$.

B. The 5D intermolecular vibrational Hamiltonian

To describe the 5D Hamiltonian used here for clusters containing open-shell radicals, it is best to begin with the Hamiltonian for an open-shell monomer interacting with a single closed-shell atom. This is

$$H = \hat{T} + H_{\text{mon}} + \hat{V}(R, r, \theta), \quad (1)$$

where the atom-diatom geometry is described in Jacobi coordinates (R, r, θ) . For an atom-diatom complex the kinetic energy operator \hat{T} is conveniently written as

$$\hat{T} = \hat{T}_R + \hat{\mathbf{L}}^2 = -\frac{\hbar^2}{2\mu_0 R} \frac{\partial^2}{\partial R^2} R + \frac{\hbar^2}{2\mu_0 R^2} (\hat{\mathbf{J}} - \hat{\mathbf{j}})^2, \quad (2)$$

where μ_0 is the Ar–OH reduced mass, \mathbf{J} is the total angular momentum of the complex, and $\mathbf{L} = \mathbf{J} - \mathbf{j}$ is its end-over-end rotational angular momentum. The open-shell monomer Hamiltonian H_{mon} and the intermolecular potential $\hat{V}(R, r, \theta)$ are described in more detail below.

Because of the very different frequencies for the OH stretching and the intermolecular vibrations, we can perform an adiabatic separation and carry out calculations on an effective (vibrationally averaged) potential surface for each OH stretching state v . The effective Hamiltonian is then

$$H_v = \hat{T}_R + \frac{\hbar^2}{2\mu_0 R^2} (\hat{\mathbf{J}} - \hat{\mathbf{j}})^2 + \hat{V}_v(R, \theta) + H_{\text{mon}}, \quad (3)$$

where $\hat{V}_v(R, \theta)$ is the vibrationally averaged intermolecular potential for a monomer in vibrational state v .

The principal approximations made for Ar_nOH clusters in the present work are identical to those employed previously in the quantum 5D treatment of Ar_nHF clusters:^{19–21} (i) the Ar_n subunit is held fixed at its equilibrium geometry and (ii) rotation of the complex is neglected. The OH monomer is thus free to move around inside or outside the Ar_n subunit. Under these circumstances, it is convenient to use Cartesian coordinates for the center of mass of the OH molecule, but to retain angular coordinates θ and ϕ to describe its orientation. The resulting 5D Hamiltonian is then^{19–21}

$$H = -\frac{\hbar^2}{2\mu_n} \left(\frac{\partial^2}{\partial X^2} + \frac{\partial^2}{\partial Y^2} + \frac{\partial^2}{\partial Z^2} \right) + H_{\text{mon}} + \hat{V}(X, Y, Z, \theta, \phi), \quad (4)$$

where μ_n is the reduced mass of the Ar_n –OH cluster, $\mu_n = (m_{\text{Ar}_n} m_{\text{OH}}) / (m_{\text{Ar}_n} + m_{\text{OH}})$. The coordinate system is fixed with respect to the Ar cage; it is to some extent arbitrary, but some choices of coordinate system give better quantum numbers than others. Where possible, it is best to choose the Z axis to lie along the highest-order symmetry axis of the equilibrium geometry of the complex, or at least to run from the OH molecule towards a central point in the Ar_n subunit.

C. The open-shell monomer Hamiltonian

The complete effective Hamiltonian for an open-shell monomer is quite complicated, but for the current application it is adequate to use the simplified form

$$H_{\text{mon}} = E_v + b_v [\hat{J}^2 + \hat{s}^2 - \hat{s}_z^2 - \hat{j}_z^2] + a_v \hat{l}_z \hat{s}_z - b_v [\hat{J}_- \hat{s}_+ + \hat{J}_+ \hat{s}_-], \quad (5)$$

where b_v and a_v are the rotational constant and spin-orbit coupling constant for a monomer in vibrational state v . In this work, we consider OH ($X^2\Pi$) in its $v=0$ state, with $b_0 = 18.56 \text{ cm}^{-1}$ and $a_0 = -139.21 \text{ cm}^{-1}$.²³ The quantity E_v contributes a constant to the total energy of the system, and so is ignored in the following discussion.

There are additional terms in the monomer Hamiltonian that couple different electronic states and are responsible for effects such as λ doubling. These could be included if required, but are not important at the present level of accuracy.

D. The interaction potential

The interaction potential between a molecule in a Π state and a single closed-shell atom is usually characterized by two potential energy surfaces, $V_{A'}(R, \theta)$ and $V_{A''}(R, \theta)$. The corresponding electronic wave functions are even and odd, respectively, with respect to reflection in the plane of the molecule, so that the two surfaces correspond to approach of the atom along a lobe of the singly occupied π orbital, or in its nodal plane, respectively.

The interaction potential may also in principle include terms that modify the spin-orbit coupling. In practice, however, these are unknown, and they are neglected in the present work. The spin-orbit operator is thus taken to have the same form in the cluster as in the OH monomer.

In a cluster containing a molecule in a Π state and n perturbing closed-shell atoms, there are still two potential energy surfaces. However, these cannot be obtained by summing the atom-diatom potentials $V_{A'}$ and $V_{A''}$ directly, because there is in general no single molecular plane. Under these circumstances, it is easier to work with the sum and difference potentials,

$$V_0(R, \theta) = \frac{1}{2}[V_{A'}(R, \theta) + V_{A''}(R, \theta)], \quad (6)$$

$$V_2(R, \theta) = \frac{1}{2}[V_{A'}(R, \theta) - V_{A''}(R, \theta)]. \quad (7)$$

The potentials $V_\nu(R, \theta)$ ($\nu=0,2$) may be thought of as the components in an expansion

$$V(R, \theta, \chi) = \sum_\nu V_\nu(R, \theta) \exp(i\nu\chi), \quad (8)$$

where χ is an angle that describes the azimuthal position of the unpaired electron with respect to the triatomic plane. This viewpoint is useful in understanding the matrix elements between electronic functions.

In a basis set of functions with $\omega = +\frac{3}{2}, +\frac{1}{2}, -\frac{1}{2},$ and $-\frac{3}{2}$, so that $(\lambda, \sigma) = (+1, +\frac{1}{2}), (+1, -\frac{1}{2}), (-1, +\frac{1}{2})$ and $(-1, -\frac{1}{2})$ respectively, the potential due to the interaction of n Ar atoms with OH ($X^2\Pi$), $\mathbf{V}_{\text{Ar-CH}}^{\text{tot}}$, can be represented by a 4×4 matrix

$$\mathbf{V}_{\text{Ar-OH}}^{\text{tot}} = \begin{pmatrix} V_0^{\text{tot}} & 0 & V_2^{\text{tot}} & 0 \\ 0 & V_0^{\text{tot}} & 0 & V_2^{\text{tot}} \\ (V_2^{\text{tot}})^* & 0 & V_0^{\text{tot}} & 0 \\ 0 & (V_2^{\text{tot}})^* & 0 & V_0^{\text{tot}} \end{pmatrix}. \quad (9)$$

In this basis set, V_0 is diagonal and V_2 provides an off-diagonal matrix element of magnitude V_2 for each perturbing atom. The quantities V_0^{tot} and V_2^{tot} will be defined in more detail below.

The two (doubly degenerate) spin-free adiabatic potential surfaces for the cluster can be obtained by diagonalizing the matrix (9). Alternatively, two adiabatic surfaces including spin-orbit coupling may be obtained by diagonalizing $\mathbf{V}_{\text{Ar-OH}}^{\text{tot}} + \mathbf{H}_{\text{so}}$, where

$$\mathbf{H}_{\text{so}} = \begin{pmatrix} a_v/2 & 0 & 0 & 0 \\ 0 & -a_v/2 & 0 & 0 \\ 0 & 0 & -a_v/2 & 0 \\ 0 & 0 & 0 & a_v/2 \end{pmatrix}. \quad (10)$$

This is what was done in locating the equilibrium geometries of Ar_nOH clusters in Paper II. However, for bound-state calculations we need to retain both surfaces and the coupling between them, and for this purpose it is better to work in the diabatic representation.

When there are several perturbing atoms, the matrix elements of the potential are most conveniently calculated in a monomer-fixed axis system with its z axis along the OH

bond and its x axis containing one of the solvating atoms. [Note that this is not the same axis system as is used for the OH translations.] The positions of the n perturbing atoms are specified by spherical polar coordinates R_i, θ_i, χ_i for $i = 1-n$. In the present model, we take the part of the potential that is diagonal in λ , due to V_0 , to be just a simple sum over n atomic perturbers,

$$V_0^{\text{tot}} = \langle +1|V|+1 \rangle = \langle -1|V|-1 \rangle = \sum_{i=1}^n V_0(R_i, \theta_i). \quad (11)$$

However, the off-diagonal terms, due to the difference potential V_2 , depend on χ_i ,

$$V_2^{\text{tot}} = \langle +1|V|-1 \rangle = \langle -1|V|+1 \rangle^* \\ = \sum_{i=1}^n V_2(R_i, \theta_i) \exp(-2i\chi_i). \quad (12)$$

The exponential factor in Eq. (12) arises because the potential due to atom i actually contains factors $\exp(i\nu(\chi - \chi_i))$ instead of $\exp(i\nu\chi)$. Because of the phase factors, the overall effect of V_2 vanishes for any regular array of atoms with more than twofold symmetry around the z axis. In general, however, V_2^{tot} as defined here is a complex quantity, and the matrix (9) is complex Hermitian rather than real symmetric.

In the present work, we use potential energy surfaces constructed from the Ar-OH ($X^2\Pi$) surfaces of Dubernet and Hutson,⁶ assuming pairwise additivity in the sense of Eqs. (11) and (12). It may be noted that the phase factors in Eq. (12) actually make the surfaces nonadditive in the usual sense. The Ar-Ar interaction is described by the HFD-C potential of Aziz and Chen,²⁴ which has a well depth of 99.55 cm^{-1} for the equilibrium Ar-Ar distance of 3.759 \AA . Since the Ar-Ar distances are held fixed in the 5D calculations, the Ar-Ar potential provides only an overall energy shift for each cluster.

E. Accuracy of the rigid-cage approximation

The approximation of treating the Ar_n cage or subunit as internally rigid is a good one (for the modes involving diatom translation and rotation) as long as the structure of the Ar_n subunit does not change much as the diatomic molecule moves around. This is true for Ar_nOH ($X^2\Pi$) because the interaction potential between OH and Ar is such that the OH-Ar equilibrium distance does not depend strongly on the OH orientation. In contrast, the potential between CH ($X^2\Pi$) and Ar has very different equilibrium distances for in-plane and out-of plane approach of Ar to CH, so that it would be inappropriate to treat the Ar_n subunit as rigid in Ar_nCH clusters. Taking the Ar_n cage to be rigid in Ar_nOH remains valid even though some of its isomers are separated by just several wave numbers, as discussed in Sec. III H. The barriers between these minima are on the order of 100 cm^{-1} or more, making the interconversion of isomers difficult. Consequently, the Ar_n subunits are localized in their respective potential minima, justifying the rigid- Ar_n approximation.

F. Bound-state methodology

For a monomer described by Hund's case (a), the rotational states of the free molecule are described by normalized symmetric top rotational functions.^{22,25} In terms of Euler angles $(\phi, \theta, 0)$ describing the orientation of the molecule, the functions are

$$\langle \theta, \phi | j P \omega \rangle = \left(\frac{2j+1}{4\pi} \right)^{1/2} D_{P, \omega}^{j*}(\phi, \theta, 0), \quad (13)$$

where $D_{P, \omega}^{j*}(\phi, \theta, 0)$ are (complex conjugates of) Wigner rotation matrices with the phase convention of Brink and Satchler.²⁶ The quantum number P describes the projection of the diatom angular momentum onto the Z axis fixed in the cluster.

The computational methodology used here is an extension of that developed for the 5D intermolecular vibrational eigenstates of closed-shell clusters such as Ar_nHF .²¹ A 3D direct product discrete variable representation (DVR)^{27,28} is employed for the X , Y , and Z coordinates and normalized spherical top functions as in Eq. (13) are used for the angular coordinates and the electronic degree of freedom. Together, these constitute a 5D basis set $|X_\alpha\rangle|Y_\beta\rangle|Z_\gamma\rangle|jP\omega\rangle$. However, since there are two coupled potential energy surfaces involved, corresponding to an extra degree of freedom, we refer to the present calculations as five-dimensional/two-surface (5D/2S) calculations when we wish to distinguish them from the simpler 5D calculations needed in the closed-shell case.

The technical aspects of the implementation of sin DVR methods together with sequential diagonalization and truncation for the X , Y , and Z coordinates have been described previously.²¹ We have used similar procedures and the same notation for Ar_nOH ($X^2\Pi$) in the present work, with two main modifications. First, a primitive sin DVR basis has been used in place of the potential-optimized (PO) DVR method used for Ar_nHF . Second, the potential part

$\hat{V}(X, Y, Z, \theta, \phi)$ has been handled in a diabatic representation.

For Ar_nHF clusters, the PO-DVR method²⁹ was found to be efficient, reducing both memory and CPU requirements without losing accuracy.²¹ However, the accuracy of the energy levels does depend on how the reference potential that defines the PO-DVR points is chosen. In the present open-shell problem, because there are two different PESs involved, it is difficult to construct a single *effective* PES to use as the reference potential. Tests of PO-DVR approaches for Ar_nOH clusters showed poor convergence compared to a primitive (unoptimized) DVR approach. To convert the previous formulation²¹ using PO DVR to the primitive sin DVR is very simple: All reference potentials are set to zero.

The complete 5D/2S problem is solved in two stages. First, for each pair of DVR points (X_α, Y_β) , we solve a 3D eigenvalue problem in Z and the angular coordinates,

$${}^{\text{3D}}h^{\alpha\beta}|\Phi_p^{\alpha\beta}\rangle = {}^{\text{3D}}\epsilon_p^{\alpha\beta}|\Phi_p^{\alpha\beta}\rangle, \quad (14)$$

where

$${}^{\text{3D}}h^{\alpha\beta} = -\frac{\hbar^2}{2\mu_n} \frac{\partial^2}{\partial z^2} + \hat{V}(X_\alpha, Y_\beta, z, \theta, \phi) + H_{\text{mon}} \quad (15)$$

and

$$|\Phi_p^{\alpha\beta}\rangle = \sum_{\gamma, j, P, \omega} C_{\gamma j P \omega, p}^{\alpha\beta} |Z_\gamma\rangle |jP\omega\rangle. \quad (16)$$

The monomer Hamiltonian H_{mon} has been described above. In the basis set $|jP\omega\rangle \equiv |jP\lambda\sigma\rangle$, its matrix elements are diagonal in P and independent of it. In the 5D basis set $|X_\alpha\rangle|Y_\beta\rangle|Z_\gamma\rangle|jP\omega\rangle$, they may be expressed as

$$(H_{\text{mon}})_{\alpha\beta\gamma j P \omega}^{\alpha'\beta'\gamma' j' P' \omega'} = \delta_{\alpha\alpha'} \delta_{\beta\beta'} \delta_{\gamma\gamma'} \delta_{jj'} \delta_{PP'} \times (h_{\text{mon}})_{\omega'\omega}(j), \quad (17)$$

where, for $j > \frac{1}{2}$, $(h_{\text{mon}})_{\omega'\omega}(j)$ is a 4×4 matrix of the form

$$(h_{\text{mon}})_{\omega'\omega}(j) = \begin{pmatrix} E(^2\Pi_{3/2}, j) & h_{\text{dec}}(j) & 0 & 0 \\ h_{\text{dec}}(j) & E(^2\Pi_{1/2}, j) & 0 & 0 \\ 0 & 0 & E(^2\Pi_{1/2}, j) & h_{\text{dec}}(j) \\ 0 & 0 & h_{\text{dec}}(j) & E(^2\Pi_{3/2}, j) \end{pmatrix}. \quad (18)$$

The diagonal elements $E(^2\Pi_{3/2}, j)$ and $E(^2\Pi_{1/2}, j)$ may be found by considering the diagonal part of the Hamiltonian (5),

$$E(^2\Pi_{1/2}, j) = b_v j(j+1) + \frac{1}{4} b_v - \frac{1}{2} a_v, \quad (19)$$

$$E(^2\Pi_{3/2}, j) = b_v j(j+1) - \frac{7}{4} b_v + \frac{1}{2} a_v. \quad (20)$$

The off-diagonal matrix elements in Eq. (18) arise from the rotational decoupling part of the monomer Hamiltonian,

$H_{\text{dec}} = -b_v [\hat{j}_- \hat{s}_+ + \hat{j}_+ \hat{s}_-]$. This is off-diagonal by 1 in σ and therefore in ω , but is diagonal in λ and j . Its matrix elements between monomer functions are

$$\langle \lambda \sigma j | H_{\text{dec}} | \lambda \sigma \pm 1 j \rangle = -b_v [j(j+1) - \omega(\omega \pm 1)]^{1/2} \times [S(S+1) - \sigma(\sigma \pm 1)]^{1/2}. \quad (21)$$

For a doublet state, the second factor in this equation (involving S and σ) is 1. The quantities h_{dec} occurring in Eq. (18) are therefore

$$h_{\text{dec}}(j) = -b_v[j(j+1) - \frac{3}{4}]^{1/2}. \quad (22)$$

For the case of $j = \frac{1}{2}$, only the central 2×2 block of the matrix (18) exists.

The matrix elements of the potential $\hat{V}(X, Y, Z, \theta, \phi)$ between the basis functions $|X_\alpha\rangle|Y_\beta\rangle|Z_\gamma\rangle|jP\omega\rangle$ are most conveniently calculated by first expanding the sum and difference potentials V_0^{tot} and V_2^{tot} in rotation matrices $D_{\mu\nu}^{\lambda*}$,

$$V_\nu^{\text{tot}}(X_\alpha, Y_\beta, Z_\gamma, \theta, \phi) = \sum_{\lambda\mu} V_{\mu\nu}^\lambda(X_\alpha, Y_\beta, Z_\gamma) D_{\mu\nu}^{\lambda*}(\phi, \theta, 0), \quad (23)$$

where the last argument is zero because the electronic azimuthal factor $\exp(i\nu\chi)$ is handled separately as described above. The coefficients $V_{\mu\nu}^\lambda(X_\alpha, Y_\beta, Z_\gamma)$ are given by

$$V_{\mu\nu}^\lambda(X_\alpha, Y_\beta, Z_\gamma) = \left(\frac{2\lambda+1}{4\pi}\right) \int \int D_{\mu\nu}^\lambda(\phi, \theta, 0) V_\nu^{\text{tot}} \times (X_\alpha, Y_\beta, Z_\gamma, \theta, \phi) d\phi \sin\theta d\theta, \quad (24)$$

where the total potential is evaluated from Eqs. (11) and (12) with the monomer at orientation (θ, ϕ) in the frame fixed in the cluster. As noted above, V_2^{tot} is a complex quantity because of the factors $\exp(-2i\chi)$ in Eq. (12). In this work, integrals over rotation matrices are evaluated as described by Leforestier.³⁰ At each DVR grid point $(X_\alpha, Y_\beta, Z_\gamma)$, the potentials V_0^{tot} and V_2^{tot} are evaluated on a grid of points in θ and ϕ to project out the components $V_{\mu\nu}^\lambda(X_\alpha, Y_\beta, Z_\gamma)$.

The matrix elements of the rotation matrices $D_{\mu\nu}^{\lambda*}$ between the angular basis functions $|jP\omega\rangle$ are simply

$$\begin{aligned} \langle j'P'\omega' | D_{\mu\nu}^{\lambda*} | jP\omega \rangle &= [(2j+1)(2j'+1)]^{1/2} \\ &\times (-1)^{\mu-\nu+P-\omega} \begin{pmatrix} j' & \lambda & j \\ -\omega' & \nu & \omega \end{pmatrix} \\ &\times \begin{pmatrix} j' & \lambda & j \\ -P' & \mu & P \end{pmatrix}, \end{aligned} \quad (25)$$

where μ must be equal to $P' - P$ and ν must be equal to $\omega' - \omega$ to avoid a nonzero value for one of the Clebsch-Gordan (CG) coefficients.

From Eqs. (23)–(25), we may express the matrix elements of \hat{V} in the basis set $|X_\alpha\rangle|Y_\beta\rangle|Z_\gamma\rangle|jP\omega\rangle$ as

$$\begin{aligned} (\hat{V})_{\alpha\beta\gamma jP\omega}^{\alpha'\beta'\gamma'j'P'\omega'} &= \delta_{\alpha\alpha'} \delta_{\beta\beta'} \delta_{\gamma\gamma'} \\ &\times \langle j'P'\omega' | \hat{V}(X_\alpha, Y_\beta, Z_\gamma, \theta, \phi) | jP\omega \rangle \\ &= \delta_{\alpha\alpha'} \delta_{\beta\beta'} \delta_{\gamma\gamma'} \hat{V}_{jP\omega}^{j'P'\omega'}(X_\alpha, Y_\beta, Z_\gamma), \end{aligned} \quad (26)$$

where for grid point $(X_\alpha, Y_\beta, Z_\gamma)$ and $j > \frac{1}{2}$,

$$\hat{V}_{jP\omega}^{j'P'\omega'} = \begin{pmatrix} \bar{V}_{jP}^{j'P'}(\frac{3}{2}, \frac{3}{2}) & 0 & \bar{V}_{jP}^{j'P'}(\frac{3}{2}, -\frac{1}{2}) & 0 \\ 0 & \bar{V}_{jP}^{j'P'}(\frac{1}{2}, \frac{1}{2}) & 0 & \bar{V}_{jP}^{j'P'}(\frac{1}{2}, -\frac{3}{2}) \\ \bar{V}_{jP}^{j'P'}(-\frac{1}{2}, \frac{3}{2}) & 0 & \bar{V}_{jP}^{j'P'}(-\frac{1}{2}, -\frac{1}{2}) & 0 \\ 0 & \bar{V}_{jP}^{j'P'}(-\frac{3}{2}, \frac{1}{2}) & 0 & \bar{V}_{jP}^{j'P'}(-\frac{3}{2}, -\frac{3}{2}) \end{pmatrix}, \quad (27)$$

where

$$\begin{aligned} \bar{V}_{jP}^{j'P'}(\omega', \omega) &= \sum_{\lambda} V_{P'-P, \omega'-\omega}^\lambda(X_\alpha, Y_\beta, Z_\gamma) \\ &\times (-1)^{P'-\omega} \begin{pmatrix} j' & \lambda & j \\ -\omega' & \omega'-\omega & \omega \end{pmatrix} \\ &\times \begin{pmatrix} j' & \lambda & j \\ -P' & P'-P & P \end{pmatrix}. \end{aligned} \quad (28)$$

As before, for the case of $j = \frac{1}{2}$, only the central 2×2 block of the matrix (29) exists.

Using Eqs. (21)–(29), we may now solve Eq. (14), which describes the hindered rotation of the diatomic molecule coupled to the Z-axis vibration (against the large Ar_n subunit) in the cluster. The Hamiltonian matrix is complex Hermitian rather than real symmetric matrix in the signed- ω

basis set used here. It would in principle be possible to symmetrize the basis set to obtain a real symmetric Hamiltonian matrix, but this was not done in the present work. It may be noted that the angular basis set size for the open-shell problem is almost a factor of 4 larger for the open-shell case $\{4 \times [(j_{\text{max}} + \frac{1}{2})(j_{\text{max}} + \frac{3}{2}) - 1]\}$ than for the closed-shell case $[(j_{\text{max}} + 1)^2]$.²¹

The final step is to diagonalize the 5D Hamiltonian, using primitive sin DVR functions for the X and Y coordinates but contracted functions from the 3D calculation for the Z coordinate and the angular degrees of freedom. The contracted functions are selected by choosing a cutoff energy ${}^{3\text{D}}\epsilon_{\text{cut}}$, which is the same for every 3D cut; only those eigenvectors $|\Phi_p^{\alpha\beta}\rangle$ whose eigenvalues ${}^{3\text{D}}\epsilon_p^{\alpha\beta}$ are below ${}^{3\text{D}}\epsilon_{\text{cut}}$ are retained in the final basis set. The final equation, (4), is very similar to Eq. (18) of Ref. 21, except that now the 3D coefficients ${}^{3\text{D}}C_{\gamma j P \omega, p}^{\alpha\beta}$ are complex numbers.^{2,3} The final 5D Hamiltonian of Eq. (4) in the contracted basis set $\{|X_\alpha\rangle|Y_\beta\rangle|\Phi_p^{\alpha\beta}\rangle\}$, \bar{H} , is

$$\begin{aligned} \bar{H}_{\alpha\beta p}^{\alpha'\beta'p'} = & \delta_{\beta\beta'} \left(\sum_{n=1}^{N_X} T_{n\alpha}^X T_{\alpha'}^X \epsilon_n^X \right) \sum_{q=1}^{N_{Z,j_{\max}}} ({}^3D C_{qp}^{\alpha\beta}) * {}^3D C_{qp'}^{\alpha'\beta'} \\ & + \delta_{\alpha\alpha'} \left(\sum_{n=1}^{N_Y} T_{n\beta}^Y T_{\beta'}^Y \epsilon_n^Y \right) \sum_{q=1}^{N_{Z,j_{\max}}} ({}^3D C_{qp}^{\alpha\beta}) * {}^3D C_{qp'}^{\alpha'\beta'} \\ & + \delta_{\alpha\alpha'} \delta_{\beta\beta'} \delta_{pp'} {}^3D \epsilon_p^{\alpha\beta}. \end{aligned} \quad (29)$$

The subscript q appearing in Eq. (29) stands for indices $\{\gamma j p \omega\}$ instead of $\{\gamma j m\}$ as in Eq. (18) of Ref. 21.

G. Modifications for Δ states

The theory needed to handle solvation of an open-shell molecule in a Δ state is quite similar to that for a Π state. The major differences are in the potential energy surfaces and in the monomer Hamiltonian.

For a single atom interacting with a molecule in a Δ state, the two spin-free surfaces are both of A' symmetry and the difference potential is V_4 rather than V_2 . In a cluster, the factor $\exp(-2i\chi)$ in Eq. (12) must be replaced by $\exp(-4i\chi)$ and V_4^{tot} (which has matrix elements between $\lambda = +2$ and $\lambda = -2$) must be expanded in rotation matrices with $\nu = 4$.

For a ${}^2\Delta$ state, the diagonal elements of the monomer Hamiltonian are

$$E({}^2\Delta_{3/2}, j) = b_v j(j+1) - \frac{7}{4} b_v - a_v, \quad (30)$$

$$E({}^2\Delta_{5/2}, j) = b_v j(j+1) - \frac{13}{4} b_v + a_v, \quad (31)$$

and

$$h_{\text{dec}} = -b_v \left[j(j+1) - \frac{15}{4} \right]^{1/2}. \quad (32)$$

H. Computational aspects

The complicated forms of the potential and of the monomer Hamiltonian make the open-shell problem significantly more difficult to solve than the closed-shell one for several reasons: (i) the angular basis size is almost a factor of 4 larger than in the closed-shell case; (ii) the Hamiltonian matrices for both the 3D Hamiltonian (14) and the final 5D Hamiltonian (29) are complex in the open-shell case, but real in the closed-shell case;²¹ and (iii) the PO-DVR method cannot be easily applied in the open-shell case because of the two different PESs involved.

The primitive basis sets applied here require both enormous CPU time and large memory space. Fortunately, for clusters Ar_nOH ($X^2\Pi$) with $n \geq 4$, it nevertheless proved feasible to carry out the calculations. On fast workstations (for example, 360 MHz CPUs, 6 GB memory, and eight processors), the CPU time required varied from 150 to 500 h for the final calculation on each Ar_nOH cluster.

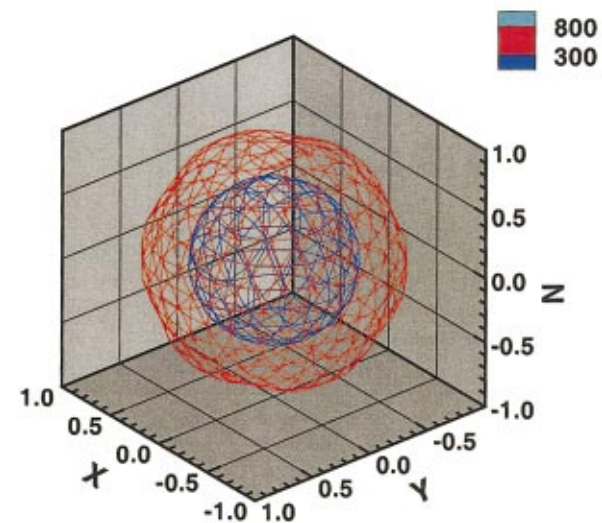
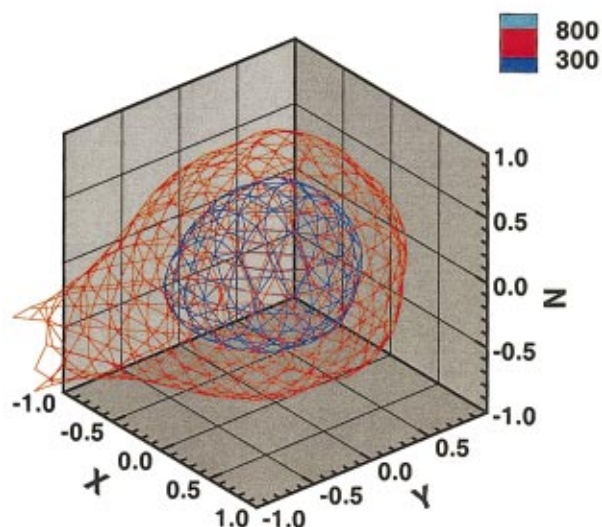
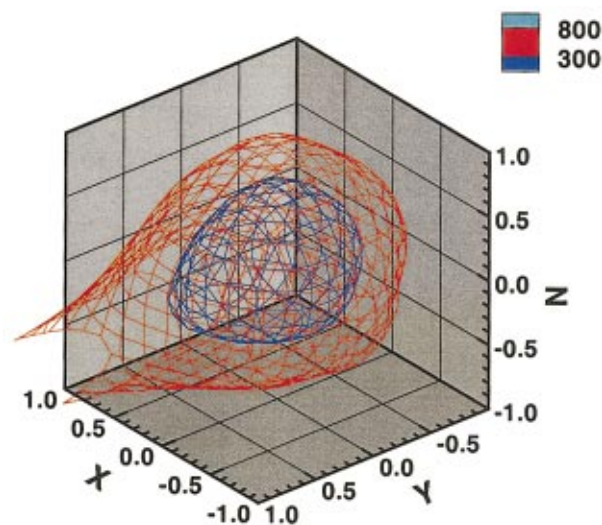


FIG. 1. (Color) Effective translational potential energy surfaces for OH ($X^2\Pi$) in Ar_{10}OH (top), in Ar_{11}OH (center), and in Ar_{12}OH (bottom). The coordinates are given in \AA .

Before carrying out convergence tests, we first examined the potential energy surface for each Ar_nOH structure for $n = 2 - 12$. For each position (X, Y, Z) of the center of mass of the OH monomer, we minimized the lower of the two PESs with

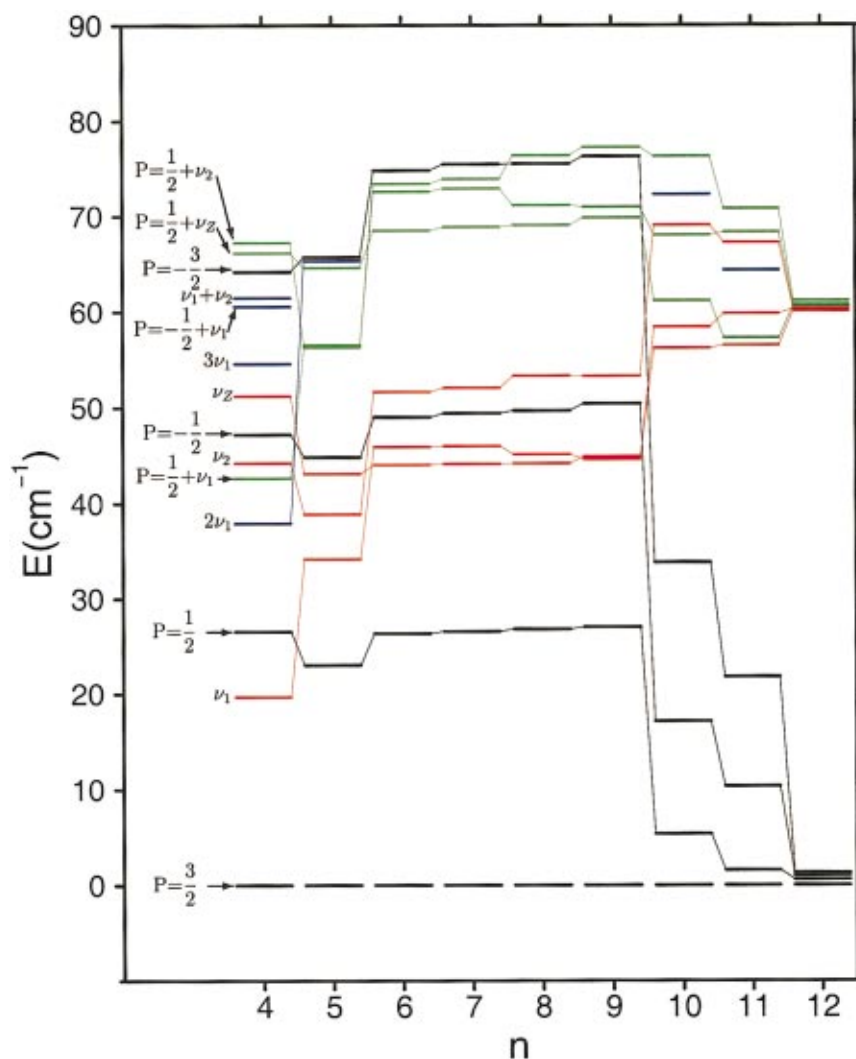


FIG. 2. (Color) The calculated level energies for the minimum-energy structures of Ar_nOH ($X^2\Pi$) complexes for $n=4-12$, shown as excitation energies from the ground state. The levels are classified as follows. Black: the four hindered rotor levels corresponding to $\text{OH } ^2\Pi_{3/2}$, $j=3/2$, $P = +3/2, +1/2, -1/2, \text{ and } -3/2$. Red: single excitations in the three translational (librational) modes from the ground state ($P = +3/2$). Green: single excitations in the three translational (librational) modes from the first excited hindered rotor state ($P = +1/2$). Blue: other levels.

respect to the orientation of the OH monomer. Examples of the resulting effective translational surfaces, for $n=10, 11$, and 12 , are shown in Fig. 1. The surfaces give us a rough idea of the spatial range of the OH translational motions. This was used as a guide in choosing the range needed for the DVR points in X, Y and Z .

For the Ar_2OH and Ar_3OH clusters, it was immediately clear from inspection of the potential surfaces that our computers could not support bound-state calculations with the present method, since the OH monomer can carry out very large amplitude translational motions and unrealistically large basis sets would be required in the primitive sin DVR approach.

The PESs for the global minimum structures of Ar_7OH , Ar_8OH , and Ar_9OH are quite similar to that for Ar_6OH , because the additional Ar atoms above Ar_6 contributes only to the second shell of atoms around OH.³ Similar PESs also exist for the global minimum structures for n from 12 to 15 . Again, the additional Ar atoms built on the Ar_{12} cage are in the second solvation shell.³

We performed convergence tests on the low-lying rovibrational energy levels for all the global minimum geometries and some low-lying isomer structures of Ar_nOH clus-

ters for $n=4-12$. Case-by-case testing is very time consuming but is necessary to obtain accurate results. Even for the same n , the rovibrational levels for different geometries generally converged at different rates. To save computer time, in some cases we permuted the (X, Y, Z) coordinates so that the lowest-amplitude motion corresponded to the Z axis. This reduced the number of DVR grid points N_Z required in solving the 3D Hamiltonian. In the end, the lowest-lying four rovibrational levels of each the Ar_nOH cluster were converged to between 0.01 and 0.05 cm^{-1} , and other levels that lie within 100 cm^{-1} of the rovibrational ground state were converged to between 0.1 and 0.2 cm^{-1} . Such accuracy is enough for us to obtain qualitative conclusions because the neglected terms in the simplified 5D Hamiltonian may lead to inaccuracies of more than 0.1 cm^{-1} in some energy levels.

For the Ar_nOH ($X^2\Pi$) problem, the rotational basis set is limited by $j_{\text{max}} = 9/2$ for all structures. The potential integrals were carried out with $N_\theta = 10$ and $N_\phi = 20$ points in θ and ϕ , respectively. Our convergence tests showed that these values give convergence to better than 0.005 cm^{-1} for all levels, which is more than adequate for present purposes.

TABLE I. The hindered rotor and spin-orbit excitation energies (in cm^{-1}) for Ar_nOH ($X^2\Pi$) clusters with $n=5-12$, at the global minimum cage geometries.

n	$\Delta E(j=\frac{3}{2}, \omega=\frac{3}{2})$			$\Delta E(j=\frac{5}{2}, \omega=\frac{3}{2})$	$\Delta E(j=\frac{1}{2}, \omega=\frac{1}{2})$	Nature of X, Y modes
	$P=+\frac{1}{2}$	$P=-\frac{1}{2}$	$P=-\frac{3}{2}$			
4	26.55	47.17	64.19	>110	>110	Cartesian
5	23.08	44.83	65.74	110.45	>120	2D circular
6	26.38	49.00	74.81	107.87	>134	2D circular
7	26.62	49.40	75.42	108.28	>135	2D circular
8	26.82	49.69	75.49	108.64	>147	Cartesian
9	27.03	50.39	76.26	108.94	>148	Cartesian
10	5.40	17.17	33.81	93.31	148.18	Cartesian
11	1.54	10.35	21.84	89.84	129.99	2D circular
12	0.56	1.03	1.31	91.24	125.78	2D circular

III. RESULTS AND DISCUSSION

The energy levels obtained from the 5D/2S calculations for cluster sizes $n=4-12$ are shown in Fig. 2, together with correlations that show how the various modes evolve with cluster size. The levels corresponding to hindered rotation of OH in the cluster are listed in Table I.

Before discussing the energy levels of Ar_nOH clusters, it is useful to recall the levels of Ar-OH itself²² and how they differ from those of closed-shell complexes.³¹ In a closed-shell complex such as Ar-HF , the HF molecule can undergo hindered rotation. In the potential due to an Ar atom, each HF rotational level with rotational quantum number j is split into components with projection $K=0,1,\dots,j$ along the intermolecular axis. In the absence of Coriolis coupling from rotation of the complex as a whole, levels that differ only in the sign of K are degenerate. Ar-OH differs in that the monomer has an electronic ground state $^2\Pi_{3/2}$, with electronic (orbital+spin) angular momentum $\omega=\pm\frac{3}{2}$ along its internuclear axis. The lowest rotational state has $j=|\omega|=\frac{3}{2}$, and is split into four components rather than two by the intermolecular potential. The pattern of energy levels has been described by Dubernet, Flower, and Hutson.²² The projection of j onto the intermolecular axis is labeled P rather than K for an open-shell complex (because K is reserved for a spin-free quantum number for Renner-Teller molecules) and the energies depend on the *sign* of P as well as its magnitude. In particular, levels in which P and ω have the *same* sign have the H of OH pointing predominantly *towards* the Ar atom, whereas those in which P and ω have *opposite* signs have the H atom pointing mostly *away* from Ar. This occurs because the OH free-rotor wave functions are Wigner rotation matrices, rather than simple spherical harmonics. The sign of P is conventionally used to designate its sign relative to ω : the lowest level thus has $P=+\frac{3}{2}$, followed by $P=+\frac{1}{2}$, $-\frac{1}{2}$, and $-\frac{3}{2}$, in that order. In Ar-OH , the four P levels arising from $^2\Pi_{3/2}$, $j=\frac{3}{2}$ are spread across 21.3 cm^{-1} , and there is also a van der Waals stretching frequency of 34.9 cm^{-1} .

A. Ar_4OH

The minimum-energy structure of Ar_4OH has C_{2v} symmetry, with the four Ar atoms on one side of OH in a “folded diamond” arrangement as shown in Fig. 5 of Paper II. The

potential felt by an OH molecule is thus not cylindrically symmetrical, so that P is not a good quantum number even when rotation of the cluster is neglected. Nevertheless, if P is defined as the projection of j onto the C_2 axis, it is still a useful label.

The results of the 5D/2S calculations for this structure are given in Table II as an example. In addition to level energies, we calculated root-mean-square vibrational amplitudes and assigned quantum numbers on the basis of wavefunction plots. As for Ar-OH itself, the ground state for Ar_4OH has $P=+\frac{3}{2}$, with OH pointing predominantly towards the “cap” of Ar atoms. The other three “internal rotation” states (with $P=+\frac{1}{2}$, $-\frac{1}{2}$ and $-\frac{3}{2}$) are spread over 64.2 cm^{-1} , with much the same pattern as in Ar-OH (the largest spacings at the bottom) but a larger spread.

In Ar_4OH , the translational motions of OH relative to Ar_4 are interleaved with the hindered rotor levels as shown in Fig. 2. Motion parallel to the “short” axis of Ar_4 (designated the Y axis here) is much easier (lower frequency) than motion parallel to the “long” axis (designated X), because the latter brings the OH into stronger repulsive interaction with the “ears” of the cap. The resulting excitation frequencies are $\nu_Y=19.68\text{ cm}^{-1}$ and $\nu_X=44.15\text{ cm}^{-1}$, respectively. Motion along the C_2 axis has an even higher frequency ($\nu_Z=51.13\text{ cm}^{-1}$) because it brings the OH molecule into direct contact with the Ar_4 subunit.

The translational quantum numbers for the ν_X , ν_Y , and ν_Z modes are designated n_X , n_Y , and n_Z , respectively. For clusters where the X and Y motions are strongly mixed (see below), ν_X and ν_Y are replaced by ν_1 and ν_2 , with quantum numbers n_1 and n_2 . For Ar_4OH , however, the X and Y motions are distinct and the wave functions for the states with $(n_X, n_Y, n_Z)=(1,0,0)$, $(0,1,0)$, and $(0,0,1)$ are shown in Fig. 3. It may be seen that the wave functions for the ν_X and ν_Y modes have clear nodal planes in the Cartesian representation. The Y translational frequency for Ar_4OH is so low that several overtones like among the lowest 14 levels shown in Fig. 2. The progression of excitation energies (37.87 , 54.54 , and 70.13 cm^{-1}) is remarkably harmonic, and the corresponding wavefunction density plots are shown in Fig. 4.

TABLE II. Results of 5D/2S bound-state calculations for Ar₄OH ($X^2\Pi$). Excitation energies are given in cm⁻¹ relative to the ground state. For this cluster, ν_1 in Fig. 2 corresponds to n_Y here. ΔX , ΔY and ΔZ are root-mean-square deviations in Å.

Level	P	(n_X, n_Y, n_Z)	Excitation energy	ΔX	ΔY	ΔZ
0	$+\frac{3}{2}$	(0,0,0)	0.00	0.16	0.23	0.15
1	$+\frac{1}{2}$	(0,1,0)	19.68	0.17	0.37	0.16
2	$+\frac{3}{2}$	(0,0,0)	26.55	0.18	0.29	0.16
3	$+\frac{1}{2}$	(0,2,0)	37.87	0.18	0.51	0.17
4	$+\frac{3}{2}$	(0,1,0)	42.58	0.18	0.35	0.21
5	$+\frac{1}{2}$	(1,0,0)	44.15	0.26	0.26	0.17
6	$-\frac{1}{2}$	(0,0,0)	47.17	0.19	0.26	0.20
7	$+\frac{1}{2}$	(0,0,1)	51.13	0.19	0.37	0.20
8	$+\frac{3}{2}$	(0,3,0)	54.54	0.18	0.62	0.19
9	$-\frac{1}{2}$	(0,1,0)	60.52	0.21	0.48	0.19
10	$+\frac{1}{2}$	(1,1,0)	61.44	0.26	0.46	0.18
11	$-\frac{3}{2}$	(0,0,0)	64.19	0.18	0.35	0.19
12	$+\frac{1}{2}$	(0,0,1)	66.11	0.20	0.34	0.23
13	$+\frac{3}{2}$	(1,0,0)	67.21	0.27	0.33	0.20

Translational levels built on the $P = +\frac{1}{2}$ excited internal rotor state may also be seen in Fig. 2, starting at 42.58 cm⁻¹ for the $P = +\frac{1}{2}$, ν_Y level.

B. Ar₅OH

The minimum-energy structure of Ar₅OH has a square pyramid of Ar atoms, with OH lying below the pyramid on the C_4 axis. As discussed previously, the Jahn–Teller distortion of the pyramid that would be expected for a $^1\Pi$ molecule is quenched by the OH spin–orbit coupling. The OH molecule thus *does* experience a cylindrically symmetrical potential, and P is a good quantum number in the absence of overall rotation of the cluster. As may be seen in Fig. 2, the four hindered rotor levels with $P = +\frac{3}{2}$, $+\frac{1}{2}$, $-\frac{1}{2}$, and $-\frac{3}{2}$ are now spread over 65.74 cm⁻¹. Again, the ground state has $P = +\frac{3}{2}$, with the H of OH pointing predominantly towards the Ar₅ subunit.

The base of the pyramid of the Ar₅ subunit is square, so there is no longer an “easy” direction for OH translational motion. Because of this, the two “in-plane” translational frequencies for OH motion are much closer together, at 34.12 and 38.81 cm⁻¹. Nevertheless, they are *not* degenerate, despite the C_{4v} symmetry. This is because there is a vibrational angular momentum $l = \pm 1$ associated with the translational motion, and Jahn–Teller states with total projection $P+l = \frac{5}{2}$ and $P+l = \frac{1}{2}$ are not degenerate. The corresponding wavefunctions are *not* appropriately labeled as ν_X and ν_Y ; they are complex linear combinations with definite values of l , and the squares of their wavefunctions are cylindrically symmetrical as shown in Fig. 5. These may be contrasted with the “Cartesian” functions with clear nodal planes obtained for Ar₄OH, and the levels are accordingly designated ν_1 and ν_2 in Fig. 2. Interestingly, the two in-plane states arising from $P = +\frac{1}{2}$ are considerably closer together than those arising from $P = +\frac{3}{2}$.

C. Ar₆OH

The minimum-energy structure for Ar₆OH has OH lying below a pentagonal pyramid of Ar atoms. The four OH hindered-rotor levels span 74.81 cm⁻¹. The two in-plane translational modes ν_1 and ν_2 are at somewhat higher frequencies than for Ar₅OH, at 45.82 and 51.60 cm⁻¹, again split by the Jahn–Teller effect. The perpendicular translation has now crossed to lower energy, $\nu_Z = 43.96$ cm⁻¹.

D. Ar_nOH, $n=7-9$

The lowest-energy structures for $n=7-9$ are built upon that for $n=6$. In all of them, the OH molecule lies below the center of a pentagonal Ar₆ pyramid, with the extra atoms added above the pyramid and out of contact with the OH. Because of this, they all have quite similar energy level patterns to Ar₆OH, as shown in Fig. 2. The only major difference is that, for $n=8$ and 9, the potential asymmetry due to the additional Ar atoms is sufficient to dominate the Jahn–Teller splitting of the in-plane translational modes referred to above, so that the corresponding wavefunctions show distinct nodal structures in Cartesian coordinates, as shown in Fig. 6, and may be identified as ν_X and ν_Y rather than ν_1 and ν_2 .

E. Ar₁₀OH

The minimum-energy structure changes dramatically for Ar₁₀OH, to one with OH at the center of an incomplete icosahedral cage of Ar atoms. Because of this, the OH molecule encounters a much less anisotropic potential than for Ar_nOH, but is translationally more strongly confined. Accordingly, the internal rotor frequencies drop as shown in Fig. 2, with the four levels with $P = +\frac{3}{2}$, $+\frac{1}{2}$, $-\frac{1}{2}$, and $-\frac{3}{2}$ now separated by only 33.81 cm⁻¹. The lowest level is still $P = +\frac{3}{2}$, with the H atom pointing predominantly towards the Ar cage (or away from the hole in the cage), but the spacings are now larger at the *top* of the group of four than at

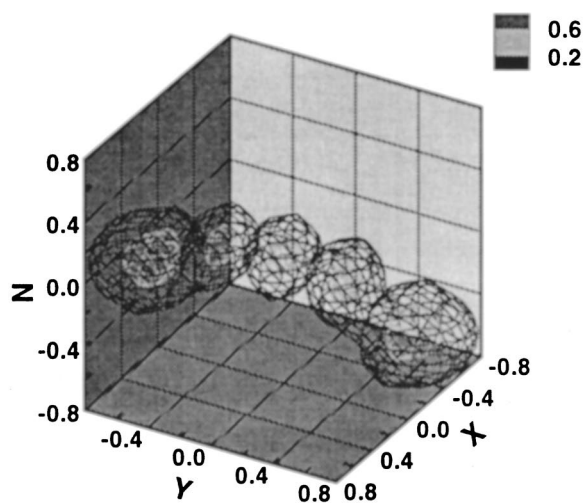
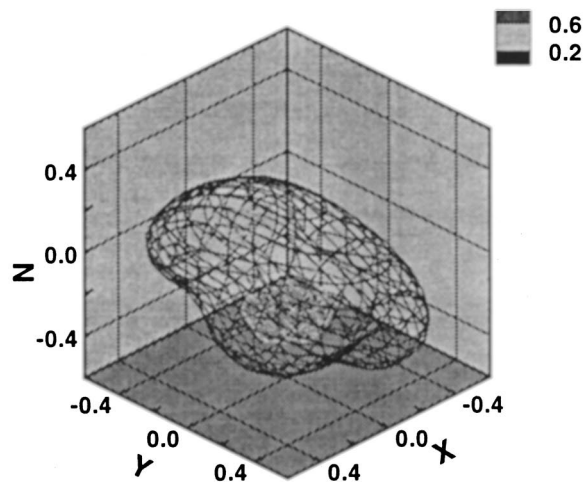
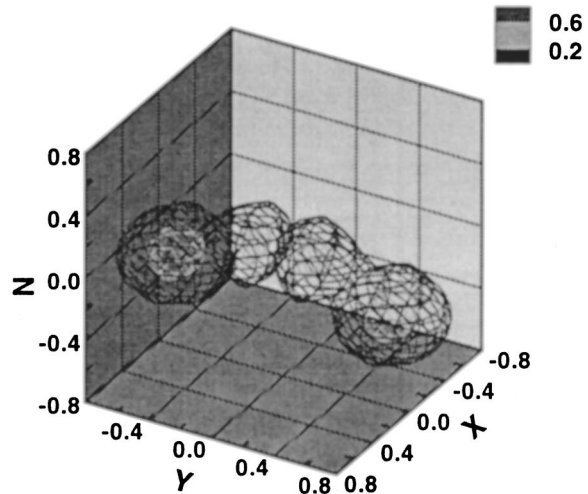
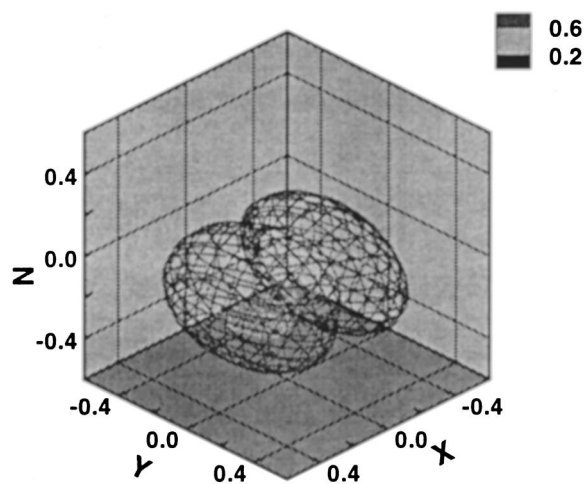
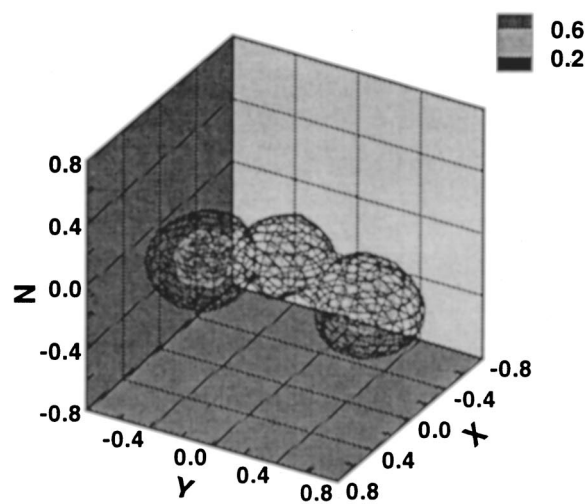
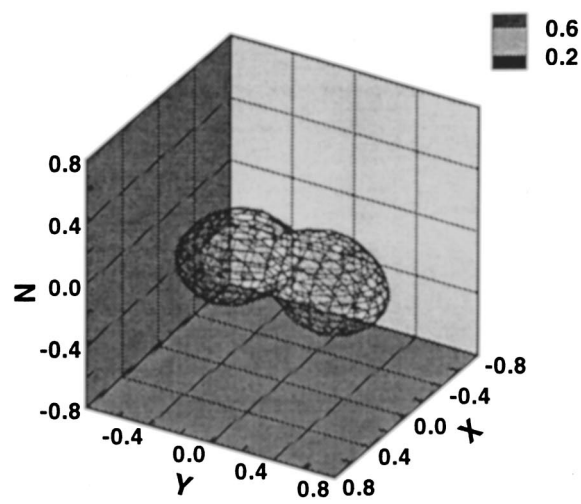


FIG. 3. The probability densities, averaged over the angular and electronic degrees of freedom, for states with one quantum of excitation in the ν_Y (top), ν_X (center), and ν_Z (bottom) translational modes for the minimum-energy structure of Ar_4OH . The corresponding excitation energies are 19.68, 44.15, and 51.13 cm^{-1} , respectively. The isosurfaces are drawn at 20% and 60%, respectively, of the maximum density. The coordinates are given in \AA .

FIG. 4. The probability densities, averaged over the angular and electronic degrees of freedom, for states with 2, 3, and 4 quanta of excitation in the low-frequency ν_Y mode for the minimum-energy structure of Ar_4OH . The corresponding excitation energies are 37.87, 54.54, and 70.13 cm^{-1} , respectively. The state with one quantum of excitation is shown in Fig. 3. The isosurfaces are drawn at 20% and 60%, respectively, of the maximum density. The coordinates are given in \AA .

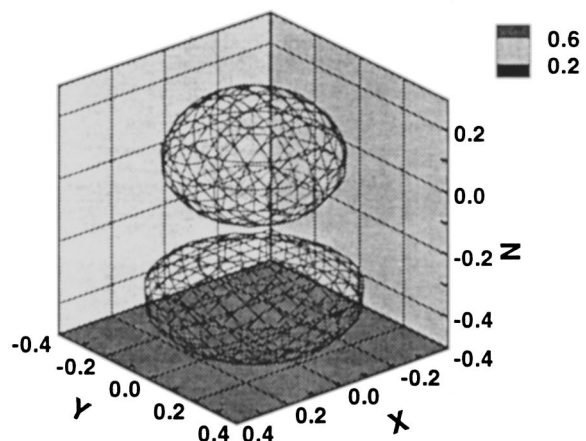
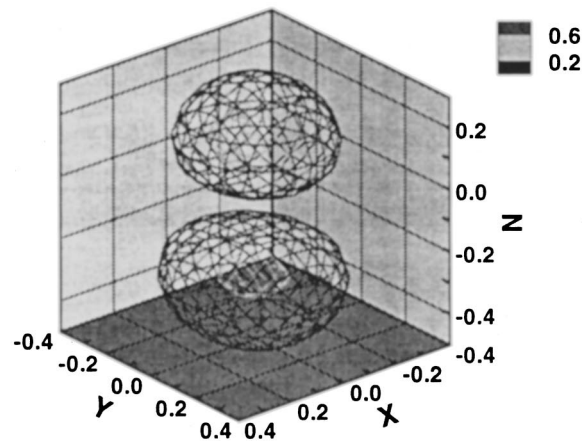
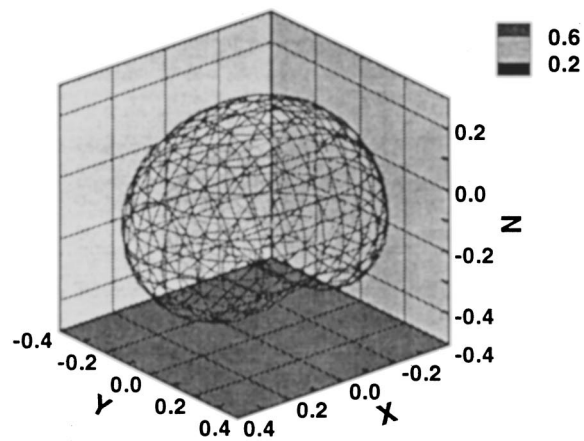
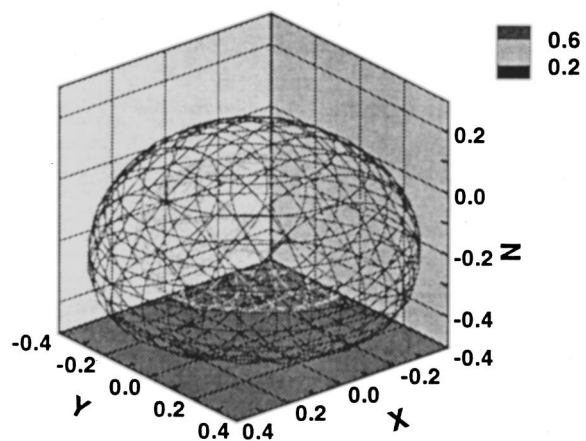
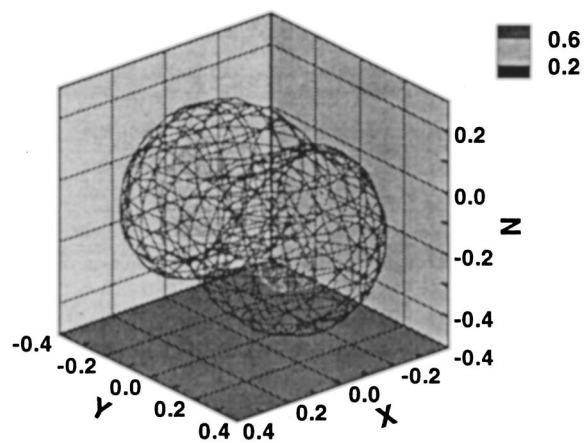
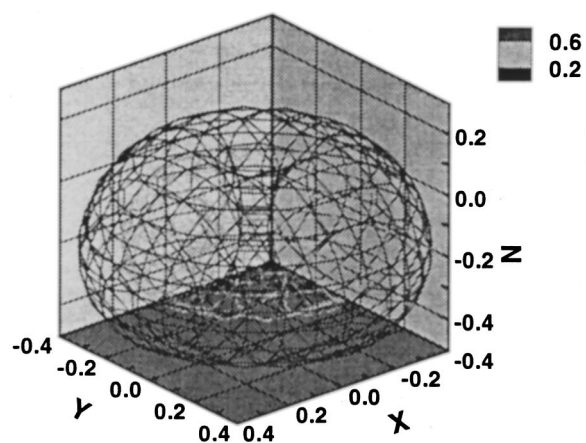


FIG. 5. The probability densities, averaged over the angular and electronic degrees of freedom, for states with one quantum of excitation in the three OH translational modes for the minimum-energy structure of Ar₅OH. The corresponding excitation energies are 34.12, 38.81, and 43.02 cm⁻¹, respectively. The mode with excitation along the Z direction (bottom) is distinct, but the other two are mixed combinations of ν_X and ν_Y with definite values of a vibrational angular momentum l , and thus have cylindrical symmetry. The isosurfaces are drawn at 20% and 60%, respectively, of the maximum density. The coordinates are given in Å.

FIG. 6. The probability densities, averaged over the angular and electronic degrees of freedom, for states with one quantum of excitation in the three OH translational modes for the minimum-energy structure of Ar₈OH. The corresponding excitation energies are 44.10, 45.06, and 53.28 cm⁻¹, respectively. Note that the X and Y modes are again distinct, in contrast with the situation for Ar₅OH shown in Fig. 5. The isosurfaces are drawn at 20% and 60%, respectively, of the maximum density. The coordinates are given in Å.

the bottom; this is inverted compared to the pattern for small numbers of Ar atoms. The in-plane translational modes are at 58.34 and 69.01 cm⁻¹, and the perpendicular mode is at 59.75 cm⁻¹.

F. Ar₁₁OH

The minimum-energy structure for Ar₁₁OH is one step further along the road to a closed icosahedral cage, now with only one vacancy. The splitting of the hindered rotor levels

TABLE III. Quantum 5D/2S vibrational ground-state energies $E_{n,i}^0$ and zero-point energies $ZPE_{n,i}$, for the global minimum ($i=1$) and the next higher isomer ($i=2$) of Ar_nOH ($X^2\Pi$) clusters. ΔV_n^2 is the difference between the equilibrium energy of the second isomer ($i=2$) and the global minimum ($i=1$) for the cluster size n . ΔE_n^2 is the difference between the quantum 5D/2S vibrational ground state energies of these two isomers. All energies are in cm^{-1} .

n	$E_{n,1}^0$	$ZPE_{n,1}$	$E_{n,2}^0$	$ZPE_{n,2}$	ΔV_n^2	ΔE_n^2
4	-890.90	98.81				
5	-1240.29	105.97	-1199.03	110.42	36.80	41.26
6	-1610.77	114.97	-1614.69	99.21	11.84	-3.92
7	-1932.05	115.52	-1920.75	123.06	3.76	11.31
8	-2349.59	116.13	-2350.47	97.84	17.41	-0.88
9	-2762.97	115.74	-2759.59	107.33	11.78	3.38
10 ^a	-3189.27	118.19	-3175.46	113.92	18.08	13.81
11	-3718.23	108.78	-3663.05	107.42	56.54	55.18
12	-4345.16	102.60	-4267.94	93.52	86.29	77.21

^aFor Ar_{10}OH , $i=3$ not 2.

thus decreases further, to 21.84 cm^{-1} , which is remarkably close to the value of 21.3 cm^{-1} found in Ar-OH . Again, though, the actual pattern is inverted compared to Ar-OH , with small spacings at the bottom and large spacings at the top. The OH translational modes are fairly similar to those in Ar_{10}OH , except that there is now very little asymmetry between the X and Y motions and the wavefunctions are again cylindrically symmetrical, with definite values of l , and are labeled ν_1 and ν_2 .

G. Ar_{12}OH

The 12th Ar atom completes the near-icosahedral cage, so that the OH molecule feels an almost spherical potential. Because of this, the four levels correlating with $j=\frac{3}{2}$ are nearly degenerate, and there is a very large spacing between these and the next group of levels at about 60 cm^{-1} , in which OH is translationally excited in the Ar_{12} cage.

The 5D/2S calculations do still give a small splitting of 1.3 cm^{-1} between the four P levels arising from $j=\frac{3}{2}$. However, this is probably an artifact of the methodology. The Ar_{12} cage structure used in the 5D/2S calculations is calculated for a fixed orientation of OH, and is thus not completely spherical. However, once the OH molecule is allowed to rotate freely, it is likely that the Ar_{12} cage will relax to reduce the barrier to internal rotation further. Under these circumstances, Coriolis coupling from overall rotation of the complex will probably destroy the P quantum number. Instead, the levels are likely to be characterized by a rotational quantum number j_{Ar} for the Ar_{12} cage as a whole, which will couple with $j=\frac{3}{2}$ to give levels with total angular momentum J from $j_{\text{Ar}}-\frac{3}{2}$ to $j_{\text{Ar}}+\frac{3}{2}$. In principle, there may also be a vibrational angular momentum l arising from the 3D translational motion of OH inside the cage.

H. Effect of zero-point energy on isomer stabilities

As described in Paper II, the potential surfaces for many of the Ar_nOH clusters have low-lying secondary minima. Where these involve different arrangements of the Ar atoms about OH (rather than just a different OH orientation), they correspond to structural isomers of the clusters. Different isomers may have significantly different zero-point energies, so that the energy separation or even the energy ordering can be affected, as found previously for the isomers of the Ar_nHF

clusters.²¹ The 5D/2S zero-point energies for the lowest two geometries for each cluster size are given in Table III: it may be seen that the zero-point energies for the absolute minimum geometry vary fairly smoothly, with a maximum between $n=6$ and 10, where the potential experienced by OH is most anisotropic and there is a significant angular contribution to the zero-point energy. However, the zero-point energies for higher-energy structures vary much more erratically, and in some cases are significantly lower. For $n=6$ and 8, the difference in 5D/2S zero-point energies is large enough to bring the isomer with the larger potential energy below the one corresponding to the absolute minimum on the potential. This is because, in each case, the second minimum involves an Ar_n subunit that is based on the Ar_4 “folded diamond” rather than the Ar_5 pentagonal pyramid, and the low ν_Y frequency that results reduces the 5D/2S zero-point energy significantly. However, it should be remembered that polytetrahedral Ar_n subunits are themselves stiffer and have higher zero-point energies than looser assemblies such as those based on a pentagonal pyramid, so that inclusion of the zero-point energy of the Ar_n might well restore the preference for the isomer corresponding to the equilibrium geometry. This was found to be the case in the recent diffusion Monte Carlo calculations on the low-lying isomers of the Ar_nHF clusters for $n \leq 7$.³² Accordingly, we have focused on the isomers with the lowest potential energy in the present paper.

IV. CONCLUSIONS

We have developed a method for quantum dynamical bound-state calculations on clusters containing an open-shell molecule solvated by n closed-shell atoms, and have applied it to Ar_nOH ($X^2\Pi$) clusters for $n=4-12$. The OH molecule is allowed to undergo hindered rotations and translations in the field of a fixed-geometry Ar_n cage or subunit. Both potential energy surfaces arising from the $^2\Pi$ state of OH are included, as well as the coupling between them. The resulting five-dimensional/two-surface (5D/2S) problem is solved using a discrete variable representation for the OH translational motions and a finite basis representation for the OH rotations and electronic structure. Spin-orbit effects are included.

The pattern of OH hindered rotor levels found in clusters is similar to that for Ar–OH itself, though extended over three to four times the energy range for $n=4-9$. The pattern changes abruptly for $n=10$, where the OH atom moves inside an Ar cage. Ar₁₂OH has a nearly spherical shell of Ar atoms around the OH, so the anisotropic splitting is very small. For $n=10$ and 11, the anisotropy may be viewed as arising from holes in an otherwise spherical shell of Ar atoms, and the resulting patterns of hindered rotor levels are inverted versions of those for Ar₂OH and Ar–OH.

The translational motions also show interesting features. For Ar₄OH, there is one direction of motion that is very weakly hindered, and a long progression of low-energy vibrations is observed. For larger clusters, the OH translational motions move to higher and higher frequency, reaching around 60 cm⁻¹ for Ar₁₂OH. Two distinct types of translational motion are observed: If the potential experienced by OH is very nearly cylindrical, as for $n=5-7$ and $n=11$ and 12, the modes for motion in the X and Y directions couple to form combinations with definite vibrational angular momentum about the Z axis, and the corresponding wavefunctions appear circular in the XY plane. However, when the OH molecule experiences a significantly noncylindrical potential, as for $n=4$ and $n=8-10$, the vibrational angular momentum is quenched and the wavefunctions have nodes in the XZ and YZ planes.

ACKNOWLEDGMENTS

Z.B. and M.X. have been supported in part by the National Science Foundation. Z.B. and M.X. also acknowledge the donors of the Petroleum Research Fund, administered by the ACS, for partial support of this research. J.M.H. is grateful to JILA, University of Colorado, and National Institute of Standards and Technology for hospitality during his Visiting Fellowship in 2001–2002.

- ¹S. Liu, Z. Bačić, J. W. Moskowitz, and K. E. Schmidt, *J. Chem. Phys.* **100**, 7166 (1994).
- ²M. Xu, Z. Bačić, and J. M. Hutson, *Faraday Discuss.* **118**, 405 (2001).
- ³M. Xu, Z. Bačić, and J. M. Hutson, *J. Chem. Phys.* **117**, 4777 (2002).
- ⁴M. H. Alexander, S. Gregurick, P. J. Dagdigan, G. W. Lemire, M. J. McQuaid, and R. C. Sausa, *J. Chem. Phys.* **101**, 4547 (1994).
- ⁵A. D. Esposti and H. J. Werner, *J. Chem. Phys.* **93**, 3351 (1990).
- ⁶M. L. Dubernet and J. M. Hutson, *J. Chem. Phys.* **99**, 7477 (1993).
- ⁷J. Klos, G. Chalasinski, M. T. Berry, R. A. Kendall, R. Burcl, M. M. Szczesniak, and S. M. Cybulski, *J. Chem. Phys.* **112**, 4952 (2000).
- ⁸M. C. Heaven, *Annu. Rev. Phys. Chem.* **43**, 283 (1992).
- ⁹W. M. Fawzy and M. C. Heaven, *J. Chem. Phys.* **89**, 7030 (1988).
- ¹⁰M. T. Berry, M. R. Brustein, J. R. Adamo, and M. I. Lester, *J. Phys. Chem.* **92**, 5551 (1988).
- ¹¹M. T. Berry, M. R. Brustein, and M. I. Lester, *J. Chem. Phys.* **90**, 5878 (1989).
- ¹²W. M. Fawzy and M. C. Heaven, *J. Chem. Phys.* **92**, 909 (1990).
- ¹³M. T. Berry, M. R. Brustein, and M. I. Lester, *J. Chem. Phys.* **92**, 6469 (1990).
- ¹⁴M. T. Berry, M. R. Brustein, and M. I. Lester, *Chem. Phys. Lett.* **178**, 301 (1991).
- ¹⁵M. T. Berry, R. A. Loomis, L. C. Giancarlo, and M. I. Lester, *J. Chem. Phys.* **96**, 7890 (1992).
- ¹⁶Y. Ohshima, M. Iida, and Y. Endo, *J. Chem. Phys.* **95**, 7001 (1991).
- ¹⁷R. T. Bonn, M. D. Wheeler, and M. I. Lester, *J. Chem. Phys.* **112**, 4942 (2000).
- ¹⁸K. Nauta and R. E. Miller, *J. Chem. Phys.* **115**, 10138 (2001).
- ¹⁹Z. Bačić, *J. Chem. Soc., Faraday Trans.* **93**, 1459 (1997).
- ²⁰S. Liu, Z. Bačić, J. W. Moskowitz, and K. E. Schmidt, *J. Chem. Phys.* **101**, 10181 (1994).
- ²¹S. Liu, Z. Bačić, J. W. Moskowitz, and K. E. Schmidt, *J. Chem. Phys.* **103**, 1829 (1995).
- ²²M. L. Dubernet, D. Flower, and J. M. Hutson, *J. Chem. Phys.* **94**, 7602 (1991).
- ²³K. P. Huber and G. Herzberg, *Molecular Spectra and Molecular Structure. IV. Constants of Diatomic Molecules* (Van Nostrand Reinold, New York, 1979).
- ²⁴R. A. Aziz and H. H. Chen, *J. Chem. Phys.* **67**, 5719 (1977).
- ²⁵R. N. Zare, *Angular Momentum: Understanding Spatial Aspects in Chemistry and Physics* (Wiley, New York, 1988).
- ²⁶D. M. Brink and G. R. Satchler, *Angular Momentum*, 2nd ed. (Clarendon, Oxford, 1968).
- ²⁷M. Mandziuk and Z. Bačić, *J. Chem. Phys.* **98**, 7165 (1993).
- ²⁸Z. Bačić and J. C. Light, *Annu. Rev. Phys. Chem.* **40**, 469 (1989).
- ²⁹J. Echave and D. C. Clary, *Chem. Phys. Lett.* **190**, 225 (1992).
- ³⁰C. Leforestier, *J. Chem. Phys.* **101**, 7357 (1994).
- ³¹J. M. Hutson, *Adv. Mol. Vibrat. Collision Dyn.* **1A**, 1 (1991).
- ³²H. Jiang, M. Xu, and Z. Bačić (unpublished).